Sliding charge density wave in the monophosphate tungsten bronze (formula presented) with alternate stacking of (formula presented) and (formula presented) (formula presented) layers

P. Foury-Leylekian, E. Sandré, S. Ravy, J.-P. Pouget, E. Elkaim, P. Roussel, D. Groult, Ph. Labbé

To cite this version:

P. Foury-Leylekian, E. Sandré, S. Ravy, J.-P. Pouget, E. Elkaim, et al.. Sliding charge density wave in the monophosphate tungsten bronze (formula presented) with alternate stacking of (formula presented) and (formula presented) (formula presented) layers. Physical Review B: Condensed Matter and Materials Physics (1998-2015), 2002, 66 (7), pp.1-16. ⟨10.1103/PhysRevB.66.075116⟩. ⟨hal-04897601⟩

Sliding charge density wave in the monophosphate tungsten bronze $(PO_2)_4(WO_3)_{2m}$ with alternate stacking of m=4 and m=6 WO3 layers

P. Foury-Leylekian, E. Sandré, S. Ravy, and J.-P. Pouget
Laboratoire de Physique des Solides, CNRS UMR 8502, Baˆtiment 510, Université Paris-sud, 91405 Orsay Cedex, France
E. Elkaim
LURE, CNRS-UMR 130, baˆt. 209D, Universite´ Paris-sud, 91405 Orsay Cedex, France
P. Roussel
Laboratoire de Cristallochimie et Physicochimie du Solide, CNRS UPRESA 8012, 59652 Villeneuve d'Ascq, France
D. Groult, and Ph. Labbe
Laboratoire CRISMAT, CNRS-UMR 6508, ISMRA-Universite´ de Caen, 14050 Caen Cedex, France

PHYSICAL REVIEW B **66**, 075116 (2002)

Sliding charge density wave in the monophosphate tungsten bronze $(\mathrm{PO}_2)_4(\mathrm{WO}_3)_{2m}$ with alternate stacking of $m=4$ and $m=6$ WO_3 layers

P. Foury-Leylekian, E. Sandré, S. Ravy, and J.-P. Pouget
Laboratoire de Physique des Solides, CNRS UMR 8502, Bâtiment 510, Université Paris-sud, 91405 Orsay Cedex, France

E. Elkaim
LURE, CNRS-UMR 130, bât. 209D, Université Paris-sud, 91405 Orsay Cedex, France

P. Roussel
Laboratoire de Cristallochimie et Physicochimie du Solide, CNRS UPRESA 8012, 59652 Villeneuve d'Ascq, France

D. Groult, and Ph. Labbé
Laboratoire CRISMAT, CNRS-UMR 6508, ISMRA-Université de Caen, 14050 Caen Cedex, France

(Received 4 January 2002; revised manuscript received 15 August 2002; published 23 August 2002)

The monophosphate tungsten bronzes $(\mathrm{PO}_2)_4(\mathrm{WO}_3)_{2m}$ form family of two-dimensional metals which exhibit charge density wave (CDW) instabilities. These materials are generally built by the regular stacking of (a,b) layers in which chains made of segments of m WO_6 octahedra directed along the **a** and $\mathbf{a}\pm\mathbf{b}$ directions are delimited. Their electronic structure thus originates from quasi-one-dimensional (1D) bands located on these chains. As a consequence their Fermi surface (FS) exhibits large flat portions whose nesting gives rise to successive CDW instabilities. Here we present a structural study of the CDW instability of the $(\mathrm{PO}_2)_4(\mathrm{WO}_3)_{10}$ member formed by the alternate stacking of layers built with segments of $m=4$ and $m=6$ WO_6 octahedra. Its *ab initio* electronic structure calculation shows that the FS of this member exhibits large flat portions which can be extremely well nested. Its best nesting wave vector accounts for the modulation wave vector stabilized by the CDW transition which occurs at 156 K. Because of the regular stacking of layers of different m values the FS is slightly split. The unusual thermal dependence of the x-ray satellite intensity provides evidence that the two types of layers become modulated at different temperature. This also leads to a slight thermal sliding of the CDW-nesting modulation wave vector, which can be accounted for within the framework of a Landau-Ginzburg theory. In addition, the observation of a global hysteresis in the thermal cycling of the satellite intensity, as well as the degradation of the interlayer order upon cooling, suggest the formation of a disordered lattice of dilute solitons. Such solitons allow to accomodate the charge transferred between the two types of layer. Finally the relevance of local charge transfers, at intergrowth defects, for example, to create pinned discommensurations that break the CDW coherence is emphasized in this whole family of bronzes.

DOI: 10.1103/PhysRevB.66.075116 PACS number(s): 71.45.Lr, 71.18.+y, 61.10.−i

I. INTRODUCTION

A. Generalities

Because of their unconventional electronic, magnetic, and structural properties transition metal bronzes and oxides are extensively studied.[1–3] Such original features originate from the possibility to obtain partial oxidation states of the transition metal (M) in an anisotropic structure built with MO_n ($n=4$, 5, 6) entities between which there is an anisotropic overlap of the t_{2g} transition-metal electronic levels. Among these compounds the spin gap vanadates $A\mathrm{V}_2\mathrm{O}_5$,[4] where A is a monovalent metal, and the molybdenum bronzes and oxides[1] have been particularly studied. The quasi-one-dimensional (quasi-1D) bronzes such as the vanadates exhibit charge localization effects, while the blue bronze $\mathrm{K}_{0.3}\mathrm{MoO}_3$ is a quasi-1D conductor presenting a charge density wave (CDW) -Peierls ground state.[1] In the CDW ground state the electronic density is modulated with the $2k_F$ wave vector (k_F is the Fermi wave vector of the 1D electron gas). CDW's are observed among the low-dimensional metals and especially in quasi-1D electronic systems, due to the strong nesting property of their Fermi surfaces (FS's) by the above quoted $2k_F$ wave vector. In this respect the study of the quasi-2D compounds is particularly interesting because their electronic structure is intermediate between that of the unconventional quasi-1D systems and that of the more conventional 3D metals. Currently only few quasi-2D systems exhibiting CDW transitions have been discovered. Besides the transition-metal dichalcogenides studied in the early 1970s, CDW instabilities have only been reported in the molybdenum purple bronzes $A\mathrm{Mo}_6\mathrm{O}_{17}$ and in molybdenum oxide $\mathrm{Mo}_4\mathrm{O}_{11}$.[1] However, the CDW instability of the 2D Mo compounds has been explained by a hidden nesting mechanism, which stabilizes the critical wave vector connecting differently oriented 1D portions of the FS.[5]

Recently, the observation of successive CDW transitions in a series of quasi-2D conductors, the monophosphate tungsten bronzes (MPTB), $(\mathrm{PO}_2)_4(\mathrm{WO}_3)_{2m}$ ($m=4$–14), has renewed interest in 2D inorganic conductors.[2,3] The MPTB's are built by stacking along the **c*** direction of (a,b) ReO_3-type layers of corner sharing WO_6 octahedra.[6] The width of these layers, which are made of elementary segments of m WO_6 octahedra, increases with m. Each WO_3 layer is isolated from the next one by a slab of phosphor

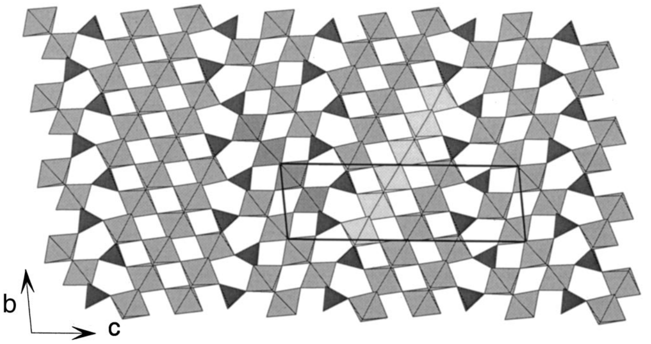

FIG. 1. Structure of $P_4W_{10}O_{38}$ showing the alternation of layers of $m=4$ and $m=6$ WO_6 octahedra in the $\mathbf{c}^*$ direction.

tetrahedra (PO_4). The connection between the PO_4 and the WO_3 slabs creates pentagonal tunnels giving the name of monophosphate tungsten bronze with pentagonal tunnels (MPTBP's) to the series. If one discards the presence of stacking defects (the occurrence of which increases with m) most of the MPTBP's are made of a regular stacking of identical layers. However, if two successive WO_3 layers are identical from a chemical point of view, their crystallographic orientation differs. There are two layers per unit cell whose orientations are related by a ''2_1'' screw axis symmetry if m is even, or by a ''n'' glide plane symmetry, if m is odd. These regular members will be noted m/m below. However, in the specific case of $P_4W_{10}O_{38}$, the most stable crystalline phase consists in an alternate stacking along $\mathbf{c^*}$ of $m=4$ and $m=6$ conducting layers (see Fig. 1).[7] In this member, noted $m/m=4/6$ below, the $m=4$ and $m=6$ layers are not related by symmetry. It is only recently that the less stable $m/m=5/5$ regular member has been synthesized and that its physical properties have been studied.[8]

In the MPTBP's, each PO_4 unit gives one electron to the WO_3 layers, which leads to an average oxidation state of $6\text{-}2/m$ for the tungsten atom. Due to the layered structure, these bronzes are quasi-2D conductors, with $(2m)(2/m)=4$ conduction electrons per unit cell containing two WO_3 layers. In the regular members made of identical layers, each layer accomodates two electrons per (a,b) area containing a single segment of m octahedra. This number must deviate from 2 in the 4/6 member, because the $m=4$ and $m=6$ layers are not related by symmetry.

Previous extended Huckel[9] and *ab initio*[10] band-structure calculations have shown that the electronic structure of the regular m/m members exhibits a hidden 1D anisotropy. In this respect the conducting layer can be decomposed into three different arrays of chains directed along the **a** and $\mathbf{a}\pm\mathbf{b}$ directions. Along each chain direction there is a strong overlap of a given combination of the three t_{2g} orbitals of the tungsten atoms in an octahedral environment. Each chain is constituted of segments of m WO_6 octahedra tilted with respect to its running direction. Because of the strong directionality of the t_{2g} orbitals, there is a weak coupling between neighboring parallel chains, which leads to the 1D anisotropy. The hidden one dimensionality also appears on the topology of the FS: the global FS of the regular members can be decomposed into three pairs of quasiplanar sheets or quasi-1D FS's. Each quasi-1D FS can be associated with one set of parallel and weakly coupled chains. A similar decomposition of the layered structure into three sets of chains has been performed in the purple bronzes and in Mo_4O_{11} (Refs. 5 and 9) and the prediction that their global FS is the superimposition of quasi-1D FS's has been recently confirmed by photoemission studies.[11]

TABLE I. Critical temperatures T_{ci} and critical wave vectors $\mathbf{q}_i$ for the small-m members of the $(PO_2)_4(WO_3)_{2m}$ family.

Member	T_c (K)	q_i
$m=4$	$T_{c1}=80\ (\pm1)$	$q_1=(0.333(5),0.295(5),0)$
	$T_{c2}=52(\pm1)$	$q_2=(0.340(5),0.000(5),0)$
$m=5$	$T_{c1}=83(\pm5)$	$q_1=(0.32(1),0.29(1),0.0(1))$
	$T_{c2}=60(\pm2)$	$q_2=(0.36(1),0.00(5),0.0(1))$
$m=6$	$T_{c1}=120(\pm1)$	$q_1=(0.385(5),0.000(5),0)$
	$T_{c2}=62(\pm1)$	$q_2=(0.310(5),0.295(5),?)$
	$T_{c3}=30$	$q_3=(0.29(2),0.11(2),?)$

B. An overview of the physical properties of the regular MPTBP's

The physical properties of the MPTBP have been previously investigated by combined electronic and structural measurements. In all the m/m members with $4\leqslant m\leqslant 14$, one or several phase transitions have been observed with, however, characteristics that strongly depend on the m value of the member.[2,3].

For the members with $m=4$, 5 (6), two (three) CDW transitions are observed.[12–14]. Their critical wave vectors and Peierls transition temperatures (T_c) are given in Table I.[8] At these transitions the transport properties exhibit singularities in their thermal dependence, and a gap appears in the magnetic susceptibility. These transitions involve the three sets of chains previously quoted. Indeed, x-ray diffuse scattering investigations show that these chains exhibit $2k_F$ pretransitional fluctuations above T_c, which are revealed by the presence, in the reciprocal space, of diffuse sheets perpendicular to the chain directions and located at the reduced wave vector $2k_F$ away from the Bragg reflections.[12] These diffuse sheets are the fingerprints on the lattice degrees of freedom of the CDW nesting instability which connects the quasi-1D portions of the FS. At the upper CDW transition (T_{c1}) satellite reflections appear at the intersection of two sets of diffuse segments out of three, which means that the modulation involves simultaneously two types of chains. Its critical wave vector corresponds to a common nesting wave vector of two sets of quasi-1D FS's associated with these chains. The lower CDW transition (T_{c2}) occurs in order to nest the remaining part of the quasi-1D FS and the electron and hole pockets which are formed at the T_{c1} transition. These findings agree with the previously quoted hidden nesting scenario,[5] which has been invoked to explain the CDW transitions of the quasi-2D molybdenum oxides and bronzes. Table I shows that for the three low-m members ($m=4$, 5, 6) the CDW transitions occur at about similar critical temperatures: T_{c1} ranges from 80 K to 120 K and T_{c2} from 50 K to 60 K. But in the $m=6$ member, the sequence of CDW transitions is reversed with respect to that of the $m=4$ and $m=5$ members. However the incommensurate components of the CDW modulation wave vectors remain very close, which means that the FS is only slightly modified from the $m=4$ to the $m=6$ member.

The members with m larger than 6 are bad metals[13–15]. At the difference of the low-m members where the conductivity sizably decreases, their electrical conductivity decreases weakly or even increases when the temperature decreases. These features indicate a tendency towards a more localized behavior of their electronic wave function. Although several CDW-like transitions with incommensurate modulations or with long period superstructures are observed in the large-m members, their CDW modulation behaves differently from that of the small-m members.[16] In particular, the detection of many harmonics shows that the modulation is strongly anharmonic, at variance with the low-m members where a sinusoidal-like modulation is observed. This nonsinusoidal character, which means that the modulation varies spatially more rapidly than for the low-m members, can be the fingerprint of a CDW built with more localized conduction electrons. The localization can be explained (1) by an enhancement of the electron-electron interactions arising from a reduction of screening effects caused by the decrease of the electronic density, or/and (2) by an increase of the electron-phonon coupling as one approaches the insulating oxide WO_3, which corresponds to the limit m infinite of the MPTBP series.

The MPTBP's of intermediate m values ($m=7{,}8$) exhibit particularly interesting phenomena. The CDW transition leads to anomalies in the charge transport properties while the magnetic susceptibility remains unaffected, which suggests a decoupling between the charge and spin degrees of freedom. In the $m=7$ member, a triply incommensurate CDW modulated state appears at a nearly first-order transition. It corresponds to the successive development of harmonics of a primary $2k_F$ modulation, which exhibit global hysteresis phenomena.[12] Interestingly, the $m=7$ member becomes also a superconductor below 0.3 K.[17] Two different types of incommensurate CDW short-range orders occur in the same temperature range in the $m=8$ member.[16] Their competition probably prevents the stabilization of a well-defined long-range CDW order. These unusual features could be due to the simultaneous presence of competing $n2k_F$ instabilities ($n=1,2,3,\dots$ in the $m=7$ member and $n=2,3$ in the $m=8$ member).

The CDW critical temperature jumps abruptly above room temperature (RT) in the $m\geqslant 9$ members. The CDW ground state stabilizes long-period superstructures in the $9\leqslant m\leqslant 12$ members and an incommensurate modulation in the $m=13$ member.[16] An additional phase transition or a short-range order for $m=10$ and 11, which leads to a doubling of the lattice periodicity along **a**, is also observed in all the $m\geqslant 9$ members. In the $m=14$ member, this last modulation (noted q_{AF} below) remains the only one observed below a high-temperature first-order phase transition. This commensurate modulation recalls the antiferroelectric (AF) order of WO_3. The relationship between the CDW and AF phenomena is supported by a recent determination of the RT CDW modulated structure of the $m=10$ member,[18] which shows that the CDW modulation itself corresponds to a ferroelectriclike shift of the W atom from the center of the WO_6 octahedra in the segment direction with an opposite phasing (i.e., AF-like phasing) between neighboring segments of the layer. In the $m=9$ members the electrical resistivity exhibits very broad humps starting at the structural transitions (see Fig. 8 in Ref. 15 for $m\geqslant 9$, Figs. 4 and 5 in Ref. 19 for $m=10$ and 12, respectively, and Fig. 2 in Ref. 20 for $m=13$) and the increase of which seems to be governed by the growth of the AF order parameter.[16]

The sharp jump of T_c from below RT, in the $m\leqslant 8$ members, to above RT, in the $m\geqslant 9$ members could be associated with the onset of the high-temperature AF instability of WO_3 with which the CDW instability seems to be coupled. This is shown, for example, by the sliding of the modulation wave vector in the $m=10$ and $m=11$ members starting from a high-temperature q_{AF} value.[16] In addition, the second-order CDW transitions of the $m\geqslant 9$ members occur without the onset of a well-defined regime of 1D fluctuations, in contrast with those exhibited by the $m\leqslant 8$ members. This means that the fluctuations are driven by short coherence length (ξ_0) effects, probably of the size of the ferroelectric segment. This behavior recalls the CDW transitions of the transition-metal dichalcogenides, which seem to be driven by local phonons.[21] In that case the phonon entropy, usually neglected in the BCS-like theory of the Peierls transition, plays a major role in the mechanism of the CDW transition. The lattice-entropy mechanism of Ref. 21 leads to a CDW with large atomic displacements achieving local chemical bondings. This is the case for the $m=10$ member, where W displacements as high as 0.2 Å are obtained in the structural refinement of Ref. 18. The lattice-entropy mechanism also implies the formation of a large Peierls gap ($2\Delta_0$) related to ξ_0 by the relationship

$$\xi_0\approx \hbar v_F/\pi\Delta_0 \tag{1}$$

(v_F is the Fermi velocity of the 1D electron gas). As the total energy is minimized (i.e., the Peierls gap is maximized), if the pattern of displacements minimizes bond-length differences between pairs of atoms, such a mechanism tends to lock the CDW to the lattice by the formation of superstructures.

The interesting feature of the MPTBP's is that whatever m, the same layered structure is maintained. With the increase of the thickness of the layer the physical properties of the MPTBP's change drastically. By stacking conducting layers with different m values, in order to induce a charge transfer between these different layers, or by inserting alkaline metals in the channels, in order to change the average conduction-electron density per layer, one expects to further modify the physical properties inside the same crystalline network. In that context several bronzes have been synthesized and are now under study. Here we present a complete investigation of one of them.

C. The $m=4/6$ alternate member

As previously mentioned, the $m/m=4/6$ bronze consists in an alternated stacking of $m=4$ and $m=6$ conducting layers. The space group of the 4/6 member is $P2_1$, with $a=5.28$ Å (binary axis direction), $b=6.56$ Å, $c=20.57$ Å, and $\alpha=96.18°$ if one uses the convention of the m/m members to label the crystallographic directions.[7] This alternate member is particularly interesting because, as the $m/m=4/4$ and $m/m=6/6$ regular members exhibit CDW instabilities with slightly different incommensurate critical wave vectors (see Table I), one expects original features coming from the competition between the CDW's issued from the m=4 and m=6 layers.

The electrical resistivity[22] of the $m=4/6$ bronze decreases almost linearly on cooling from 550 K until about 180 K. Below this temperature the resistivity stays constant until about 120 K, then the resistivity decreases progressively, more steeply below 80 K with a slope anomaly at 30 K. The resistivity of the 4/6 member does not exhibit the hump anomalies of the 4/4 and 6/6 regular members below T_{c1} and T_{c2}. A hump anomaly is, however, induced by a magnetic field of 16 T: the resistivity increases between about 180 K and 80 K (an additional very weak hump anomaly can be guessed around 150 K), then drops until 30 K, the temperature below which it further increases. The absolute value of the thermopower[22] decreases linearly with the temperature until 180 K, then its slope decreases by a factor of 2 until about 100 K, the temperature below which it further increases until 30 K. Quantum transport measurements reveal the presence of small electron and hole pockets at low temperature, and angular dependent magnetoresistance oscillations, detected below 30 K, indicate that the associated cylindrical FS is only weakly corrugated.[22]

The purpose of this paper is primarily to report an extensive x-ray investigation of the CDW instability exhibited by the $m/m=4/6$ bronze. It completes a study published in Ref. 23. The findings will be contrasted to those already obtained in the regular $m=4$, 5, and 6 members. The results will be also discussed in the light of an *ab initio* band-structure calculation, which is necessary to determine self-consistently the charge transfer between the $m=4$ and $m=6$ layers. This will enable us to account for the observed CDW critical wave vector as the one achieving the best nesting of the global FS.

II. EXPERIMENT

A. Synthesis and characterization

The study has been performed on an unique crystal prepared by the chemical vapor transport technique. A mixture of $(NH_4)_2HPO_4$ and WO_3 in appropriate proportion is first heated at 600 °C in air. Powdered metallic tungsten is then added and the medley is heated in a silica tube at 1000 °C for 2 days. In order to obtain monocrystals, the resulting polycrystalline sample is sealed in a quartz tube and placed in a furnace with a temperature gradient of 10 °C/cm (from 1200 °C to 1000 °C) for 1 week.

The crystal selected for our study was a 1 mm^2 $\times 0.3$ mm black platelet. It has been characterized by a Weissenberg method using the $\lambda_{Cu}=1.542$ Å radiation issued from a classical tube in order to measure its unit cell and to verify its crystalline quality. The measured cell parameters were those expected for the $2m=4+6$ phase and the extinction rules were compatible with those of the $P2_1$ space group. The sample was found to be of quite good quality but twinned. The twins are related by a twofold axis along the **b** direction. In the reciprocal space, the presence of twinned crystals gives rise to additional spots only along the **c*** axis direction. In this direction the Bragg reflections of the twins are separated by $\Delta l=2(b^*\cos\alpha^*/c^*)k$, k being the miller index in the **b*** direction.

B. X-ray diffuse scattering and diffraction experiments.

Preliminary results have been obtained using the $\lambda_{Cu}=1.542$ Å radiation issued from either a classical tube or a rotating anode (for the intensity measurements). All the beam lines were equipped with a doubly bent graphite monochromator. The investigation has been performed with the so-called fixed film-fixed crystal method, well adapted to detect weak diffuse scattering effects. Then the thermal dependence of the intensity of selected CDW reflections has then been measured with an Ar-NH_4 gas linear detector. Additional laboratory measurements of the position of the satellite reflections were also performed with a homemade three-circle diffractometric setup mounted on a rotating anode. The three experimental setups used were equipped with a cryocooler operating from room temperature down to 25 K.

Finally, accurate measurements of the position and the width of the satellite reflections have been performed using the Wiggler beam line DW22 at the synchrotron radiation facility of LURE. Here the beam was monochromatized by a (sagitally) focusing double crystal silicon (111) monochromator and the diffracted beam was registered on a four-circle diffractometer equipped with a cryocooler operating down to 15 K. The energy of the incoming photons was 18 KeV in order to minimize the absorption effect by the crystal. The crystal was glued with its binary axis **a** roughly aligned along the Ω axis of the diffractometer.

III. RESULTS

A. X-ray diffuse scattering investigation

1. A high-temperature modulation

X-ray experiments performed at RT and down to 200 K do not reveal the thin diffuse lines previously observed in the other regular low-*m* members of the series.[12] Only very broad diffuse trails directed along the $2\mathbf{a}^*\pm 3\mathbf{b}^*$ directions can be guessed [Fig. 2(a)]. Such diffuse trails have been already observed in almost all the MPTBP's in the same temperature range. They originate from the low-frequency vibration modes of the segments of *m* octahedra previously considered. These modes, which are uncoupled from segment to segment, correspond to an in-phase acousticlike dis-

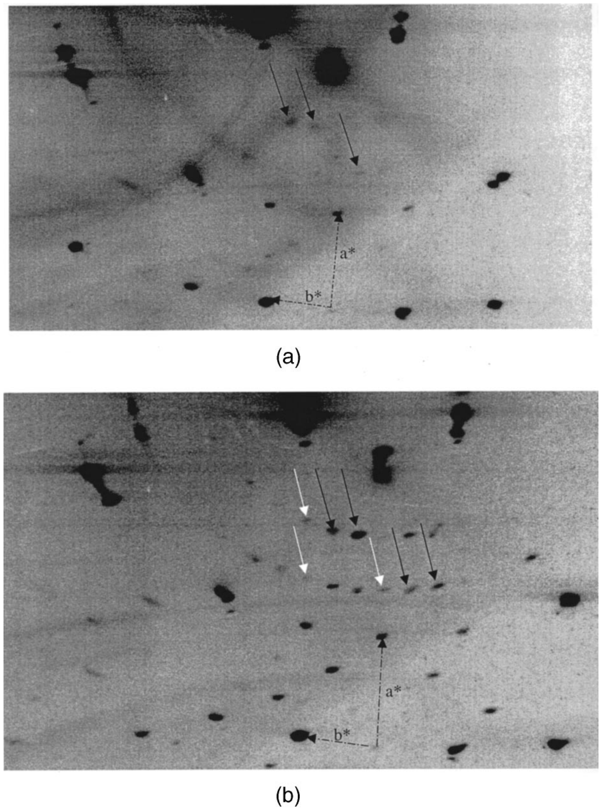

FIG. 2. X-ray patterns of the 4/6 member taken at 200 K (a) and 25 K (b). In (a) the arrows point towards the diffuse spots. In (b) the black (white) arrows point towards the $\mathbf{q}_1$ and $\mathbf{q}_2$ satellite reflections. The $\mathbf{a}^*$ and $\mathbf{b}^*$ directions are indicated.

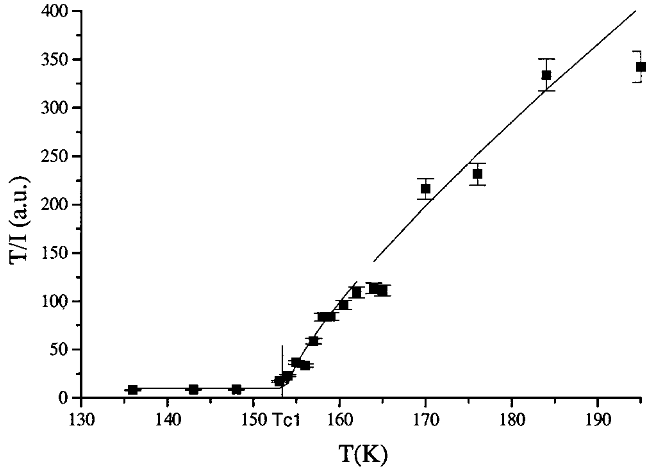

FIG. 3. Temperature dependence of the inverse peak intensity I of the $\mathbf{q}_1$ critical scattering measured at $\mathbf{Q}_1=(2,1,0)-\mathbf{q}_1$, corrected by the thermal population factor. The quantity T/I extrapolates to zero at the critical temperature T_{c1}.

placement of the m tungsten atoms of the segment, recalling the ferroelectriclike distortion of the segment previously mentioned.

Inside these diffuse trails 2D or 3D diffuse spots are detected below 220 K [see arrows on the x-ray pattern of Fig. 2(a)]. We have measured the peak intensity I of these diffuse spots as a function of the temperature T. Figure 3 gives the thermal variation of T/I below 195 K, showing clearly that it vanishes upon cooling. This means that T/I, which according to the fluctuation-dissipation theorem corresponds to the structural counterpart of the CDW susceptibility, behaves critically. The extrapolation to zero of the thermal dependence of T/I allows to expect a second-order structural transition at about 153 ± 2 K$(=T_{c1})$.

Consistently, the diffuse spots condense into well-defined satellite reflections below T_{c1}. All the satellite reflections, shown by black arrows on the x-ray pattern of Fig. 2(b), are observed at quite large diffraction angles, which is typical of a displacive structural transition. Using the laboratory diffractometric setup, the measurement of the satellite reflection position gives, with respect to the main Bragg reflection frame, a reduced wave vector of the modulation of $\mathbf{q}_1=(0.33(2),0.33(2),0.00(2))$. Within the given experimental errors $\mathbf{q}_1$ is found to have commensurate components (see below for a more accurate determination of the components). The intensity of the satellite reflections is $\approx5\times10^{-3}$ times that of an average main Bragg reflection. Satellite reflections are also detected at the $\mathbf{q}_1'=(0.33(2),-0.33(2),0.00(2))$ reduced wave vector related to $\mathbf{q}_1$ by the monoclinic symmetry of the high-temperature lattice. However at the present stage of our investigation it is not clear if $\mathbf{q}_1$ and $\mathbf{q}_1'$ belong to the same domain, which would lead to a $2q$ modulation pattern, or to two different domains, which would lead to a single q modulation pattern.

Figure 4 gives the thermal variations of the intensity of two $\mathbf{q}_1$ satellite reflections located, respectively, at the (a) $\mathbf{Q}_1=(2,1,0)-\mathbf{q}_1$ and (b) $\mathbf{Q}_2=(3,-1,-1)-\mathbf{q}_1$ reciprocal positions. The intensity of the $\mathbf{Q}_1$ reflection grows steeply below about 156 K, which is close to the temperature (T_{c1}) at which the q_1 critical scattering diverges. However Fig. 4(a) shows that the $\mathbf{Q}_1$ satellite intensity behaves nonmonotonical in temperature and that the cooling and heating cycles differ sizably below 130 K. Upon cooling, after a strong increase below T_{c1}, the intensity of the $\mathbf{Q}_1$ satellite reflection saturates between about 130 K and 100 K, then further increases, reaching a maximum around 80 K before decreasing. Upon heating, the $\mathbf{Q}_1$ intensity stays constant until 100 K, then shows a dip around 120 K, further increases until 130 K, and abruptly decreases until T_{c1}. The $\mathbf{Q}_2$ satellite intensity exhibits also a nonregular behavior in temperature and a hysteresis between the heating and cooling cycles, especially visible below 100 K. However its thermal variations, shown Fig. 4(b), differs from those of the $\mathbf{Q}_1$ reflection previously described. Upon cooling, after a weak increase below T_{c1}, the $\mathbf{Q}_2$ satellite intensity strongly increases below 125 K. Then the intensity exhibits a secondary maximum around 110 K followed by a weak dip around 90 K before a further increase below 90 K. Upon heating, the $\mathbf{Q}_2$ satellite intensity first decreases, then saturates around 100 K before decreasing, more strongly until 125 K. Then above this temperature it saturates at a weak value until T_{c1}.

In conclusion, the satellite reflection intensity exhibits, in addition to its onset at T_{c1}, anomalies in its thermal dependence around 120–130 K (T^*) and 80–100 K (T^{**}). Such unusual dependence is not exhibited by the CDW satellite

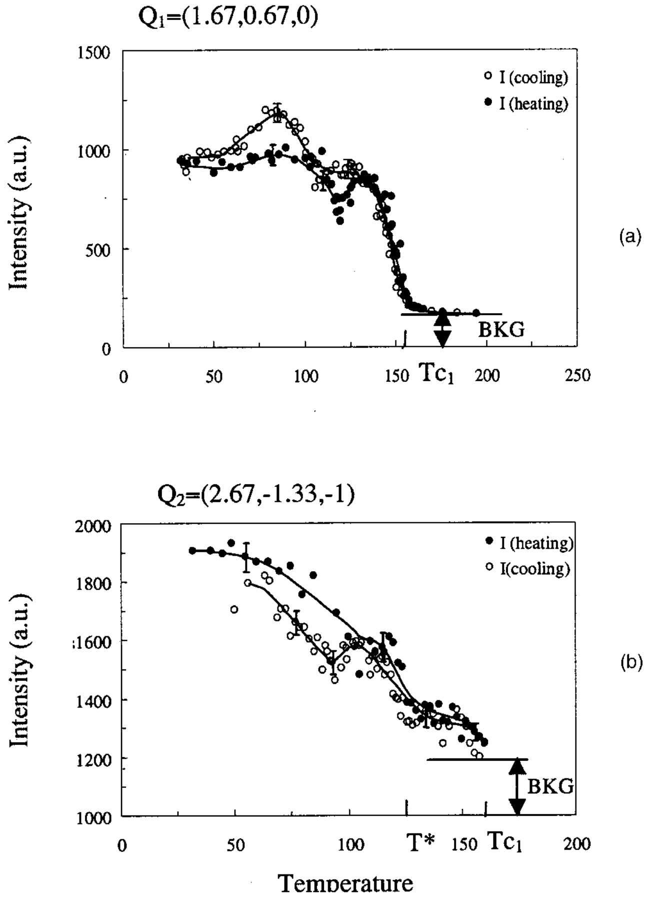

FIG. 4. Thermal dependence of the peak intensity of the $\mathbf{q}_1$ satellite reflections located at (a) $\mathbf{Q}_1=(2,1,0)-\mathbf{q}_1$ and (b) $\mathbf{Q}_2=(3,-1,-1)-\mathbf{q}_1$ reciprocal positions. The cooling and heating curves are shown by empty and full circles, respectively. T_{c1} and T^* are indicated. The background intensity (BKG) is indicated.

intensity of the regular low-m members, which increases regularly when the temperature decreases.[12] These anomalies are the fingerprints of an unconventional behavior of the CDW transition of the 4/6 member.

2. A weaker additional modulation

Another type of satellite reflection is observed at the reduced wave vector $\mathbf{q}_2=(0.33(2),0.00(2),0.00(2))$ at low temperature [white arrows on the x-ray pattern of Fig. 2(b)]. The intensity of the $\mathbf{q}_2$ satellite reflections is one order of magnitude smaller than that of the $\mathbf{q}_1$ ones. It is thus difficult to determine precisely the temperature below which the $\mathbf{q}_2$ satellite reflections appear. The photographic investigation still shows very weak $\mathbf{q}_2$ reflections at 130 K, which are not detectable at 150 K. The present investigation cannot determine if the $\mathbf{q}_2$ reflections appear at T_{c1} with an extremely weak intensity, or at a different critical temperature ($T_{c2}\simeq T^*$). In addition, one has, within experimental errors, $\mathbf{q}_2=\mathbf{q}_1+\mathbf{q}_1'$ modulo a reciprocal wave vector. Thus, one cannot exclude, if the $\mathbf{q}_1$ and $\mathbf{q}_1'$ modulations are present in the same domain, that the $\mathbf{q}_2$ modulation should be a harmonic of this modulation. However in that case one expects to detect also satellite reflections at the reduced $\mathbf{q}_3=\mathbf{q}_1-\mathbf{q}_1'$ wave vector. They have not yet been observed.

No additional structural effect has been detected until 25 K, the lowest temperature reached. This means that no structural modifications seems to occur at the temperature ~30 K at which transport properties exhibit additional anomalies.

B. Accurate measurement of the $\mathbf{q}_1$ modulation

1. Thermal variations of the modulation wave vector $\mathbf{q}_1$

The first purpose of the synchrotron experiment was to verify the commensurate value of the $\mathbf{q}_1$ reduced wave vector. For that, we have accurately recorded the intensities issued from the satellite reflection located at $\mathbf{Q}_3=(3,1,1)-\mathbf{q}_1'$ and the (8,4,3) Bragg reflection diffracted by the $\lambda/3$ wavelength (not totally eliminated by the monochromator). If $\mathbf{q}_1'$ presents commensurate (1/3,1/3,0) components, both reflections should be superimposed. At 25 K we have performed intensity scans along several reciprocal directions. We have verified that the h and l components of the satellite and of the $\lambda/3$ Bragg reflection are identical within the experimental errors. This indicates that the a^* and c^* components of $\mathbf{q}_1$ are commensurate (with a relative precision of 2×10^{-3} in reciprocal space units). But, as shown by the intensity scan of Fig. 5(a), we have observed that in the (k,l) plane the satellite reflection and the $\lambda/3$ Bragg reflection are not superimposed along $\mathbf{b}^*$. The b^* component of $\mathbf{q}_1$ is thus incommensurate: if one sets $q_{b*}=b^*/3+\Delta q_{b*}$, the shift along the k direction of the satellite reflection with respect to the $\lambda/3$ Bragg reflection is $\Delta q_{b*}=[(1.5\pm0.2)\times10^{-2}]b^*$ at 25 K. It is interesting to remark that in the regular $m=4$ member the high-temperature CDW modulation wave vector is also shifted along b^*, but in the opposite direction and with a larger amplitude than for the 4/6 member: $\Delta q_{b*}=-(3.8\times10^{-2})b^*$ (see Table I).

The same experiment has been repeated at several temperatures between 25 K and T_{c1} (Fig. 5). Only the b^* component was found with an incommensurate value at all temperatures with, however, Δq_{b*} decreasing with increasing temperature. Figure 6 shows that Δq_{b*} begins to decrease above 60K and saturates at $\Delta q_{b*}=(0.4\times10^{-2})b^*$ above 125 K. As this last shift is only twice the experimental uncertainties, one cannot exclude that $\mathbf{q}_1$ becomes commensurate in the vicinity of T_{c1}. But it is interesting to remark that $\mathbf{q}_1$ seems to vary in a limited temperature range which seems to be bounded by T^* and T^{**}, temperatures at which anomalies are observed in the thermal dependence of the satellite intensities. However as there is only one determination of Δq_{b*} performed between T^* and T^{**}, additional measurements have to be performed in order to substantiate this statement. In the regular $m=4$ bronze, recent synchrotron measurements have shown that there is not such a sliding of the incommensurate b^* component of the $\mathbf{q}_1$ modulation wave vector below T_{c1}.

2. Measure of the $\mathbf{q}_1$ *satellite reflection width*

The profile of the $\mathbf{Q}_3$ satellite reflection has been measured along the three main reciprocal directions. Along the

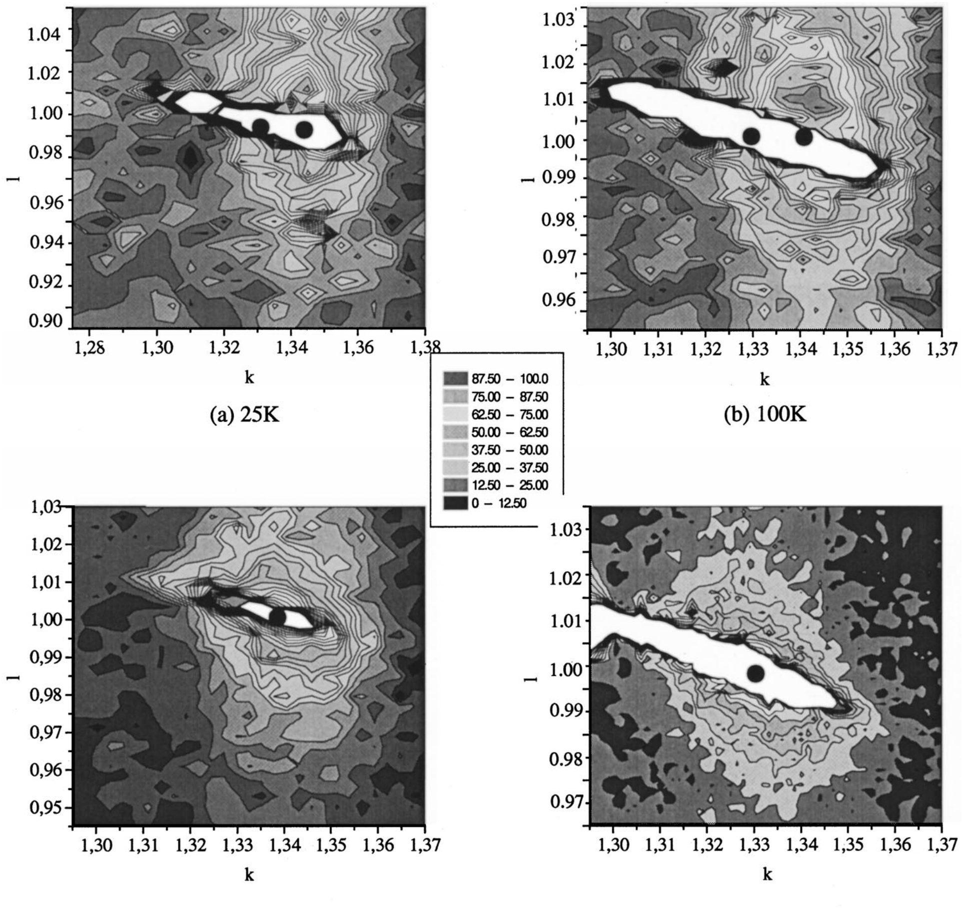

(a) 25K

(b) 100K

(c) 125K

(d) 140K

FIG. 5. Isointensity two-dimensional (k,l) map around the $\mathbf{Q}_3=(3,1,1)-\mathbf{q}_1'$ satellite reflection and the $\lambda/3$ harmonic of the (8,4,3) main Bragg reflection at (a) 25 K, (b) 100 K, (c) 125 K, and (d) 140 K. The (k,l) scale in (a) is larger than in (b)–(d). The black circles indicate the center of the reflections.

a* and **b*** directions the profile can be well fitted by a Gaussian with a width corresponding to the experimental resolution (i.e., the width of the neighboring main Bragg reflections). This means that at the scale of our experimental resolution there is a long-range CDW order in the ab layer. Along the interlayer **c*** direction, the profile of the satellite reflections can be well fitted (Fig. 7) by a Lorentzian whose width is much larger than that of the main Bragg reflections along $c*$. It is thus not necessary to perform a deconvolution of the measured profile with the experimental resolution in that direction in order to obtain the real q-space profile. The 1D Fourier transform along **c*** of this profile gives the position-position correlation function, which describes the loss of long-range order in the interlayer direction. With a Lorentzian satellite profile in the reciprocal space, one deduces that this correlation function varies as $e^{-z/l}$ in the direct space, where $l=\Delta q_{c*}^{-1}$, Δq_{c*} being the half-width at half maximum of the Lorentzian. One measures $l=520$ Å at 140 K, $l=220$ Å at 100 K, and $l=120$ Å at 25 K. These measurements surprisingly show that the CDW order deteriorates along the interlayer direction when the temperature decreases from T_{c1}. It is interesting to remark that in the regular $m=4$ member, no thermal variation of the satellite width is observed. Surprisingly, the synchrotron investigation of the $m=4$ member shows that the $\mathbf{q}_1$ satellite reflections are broader than the experimental resolution along all the reciprocal directions (**a***, **b***, and **c***).

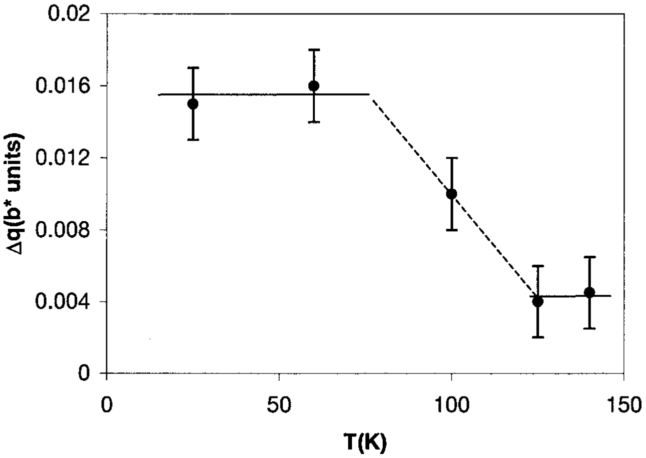

FIG. 6. Thermal variation of the splitting along **b***, Δq_{b*}, between the $\mathbf{Q}_3$ satellite reflection, and the $\lambda/3$ harmonic of the (8,4,3) main Bragg reflection.

IV. *AB INITIO* BAND-STRUCTURE AND FERMI-SURFACE CALCULATIONS

In order to perform the electronic structure calculation of the 4/6 member we have used a density-functional theory

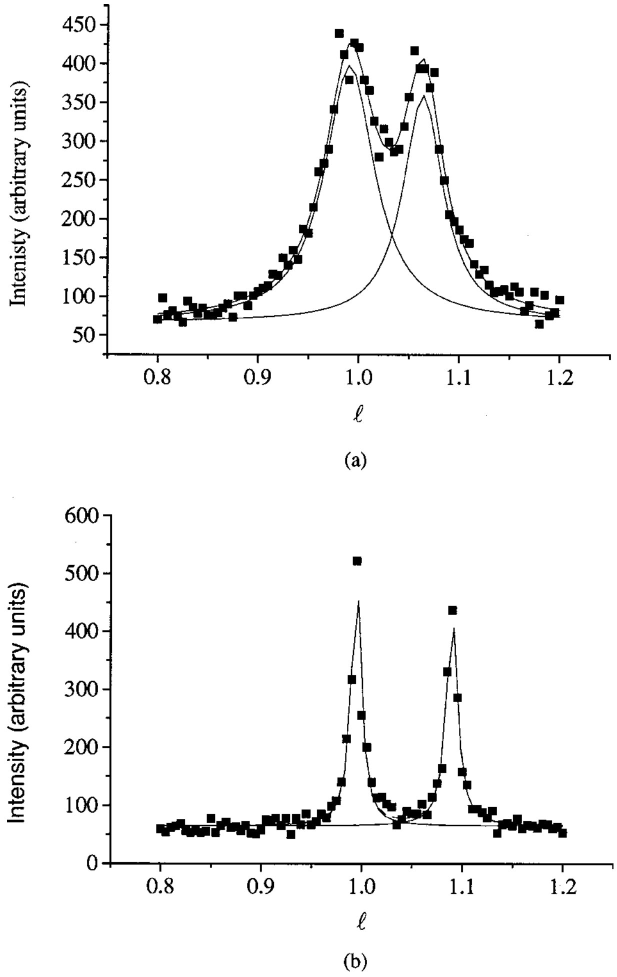

(a)

(b)

FIG. 7. Scan along $\mathbf{c}^*$ of the $\mathbf{Q}_3$ satellite reflection at (a) 25 K and (b) 140 K. The reflection located at $l=1.1$ is a satellite reflection issued from the twin. The full line is the result of a fit of the profile by a Lorentzian.

(DFT) total-energy schema[24] based on ultrasoft pseudopotentials[25] with a plane-wave basis set cutoff energy of 400 eV. The exchange and correlation energy was calculated using the local-density approximation. The conditions of calculation were identical to those used for the calculation of the electronic structure of the regular $m=4$ member.[10] This will allow a clear comparison of the band structure and of the FS between the 4/4 and 4/6 members.

The calculation gives, as expected, six conduction bands crossing the Fermi level. The energy dispersion of these bands is much less dispersive along the $\mathbf{c^*}$ direction than along the $\mathbf{a}^*$ and $\mathbf{b}^*$ directions by a factor of 50–1000 depending on the band. This means that the electron wave functions of the conduction bands are basically uncoupled from layer to layer and thus that the band structure can be viewed as the superimposition of that of the $m=4$ and $m=6$ layers. From each layer originate three bands which are mainly dispersive along the $\mathbf{a}^*$ and $\mathbf{d}^*_{\pm}$ reciprocal direction and which thus can be associated to the chains $\mathbf{a}$ ($a^*=2\pi/a$) and $\mathbf{a}\pm\mathbf{b}$ ($d^*_{\pm}=2\pi/|a\pm b|$) as for the regular members.[9,12] The bandwidth is ≈ 2 eV for the chains $\mathbf{a}$ and ≈ 1 eV for the chains $\mathbf{a}\pm\mathbf{b}$. Similar values of the bandwidth have been found in the *ab initio* calculation of the electronic structure of the regular $m=4$ member.[10] These findings agree with magnetotransport measurements[22] which show that the FS is weakly corrugated in the $\mathbf{c}^*$ direction and that the ratio of the interlayer to intralayer transfer integrals is of the order of 6×10^{-3}.

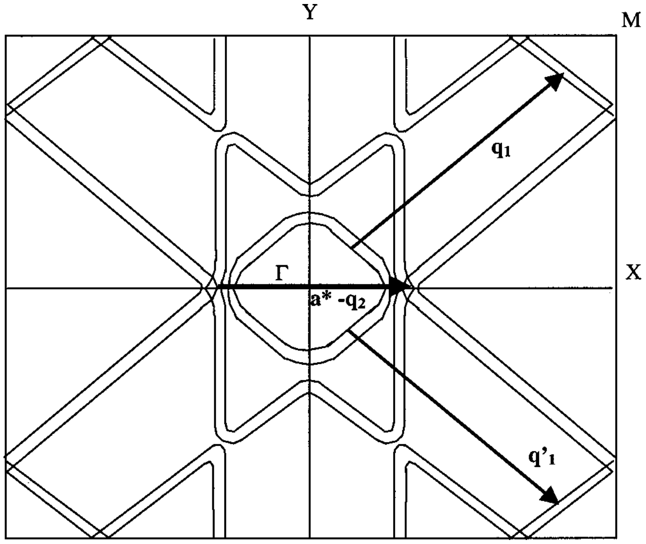

FIG. 8. Fermi surface of the 4/6 member in the $c^*=0$ plane of the Brillouin zone. The $\mathbf{q}_1$, $\mathbf{q}_1'$, and $\mathbf{q}_2$ wave vectors of the modulation are indicated.

The average conduction-band dispersion along $\mathbf{c}^*$ decreases from $\simeq 10^{-1}$ eV for the $m/m=2/2$ member (where only chains a are present) to $\simeq 10^{-2}$ eV for the $m/m=4/4$ member, then to less than 10^{-3} eV for the $m/m=4/6$ member. A straightforward explanation is that when m increases, the conduction electrons become more and more confined in the center of the layer where the WO_6 octahedra are less distorted by the presence of the PO_4 groups. This statement has been confirmed by our DFT calculation of the $m/m=4/6$ member. The calculation shows that in the $m=4$ layer the electron density, which is maximum on the two inner W atoms of the segment of four WO_6 octahedra, still spreads on the two outer W atoms in contact with the PO_4 groups, while in the $m=6$ layer there is a maximum of density on the two inner W atoms of the segment of six WO_6 octahedra and nearly no density on the two outer W atoms in direct contact with the PO_4 groups.

Figure 8 shows, in the $c^*=0$ reciprocal layer, the FS originating from the six conduction bands. As there is no substantial dispersion along $\mathbf{c^*}$, it basically gives the section of the "cylindrical" shape of the total FS. The FS clearly exhibits 1D parts perpendicular to the $\mathbf{a}^*$ and $\mathbf{d}^*_{\pm}$ reciprocal directions (i.e., respectively, parallel to the ΓY and XY directions of Fig. 8), which thus can be associated with chains $\mathbf{a}$ and $\mathbf{a}\pm\mathbf{b}$. The FS is split along these directions, as expected by the presence of uncoupled parallel chains having different filling factors in the $m=4$ and $m=6$ layers. The 1D parts of the FS are less warped and the hybridization gap between bands associated with different chains are smaller in the 4/6 member than in the 4/4 member.[10] The first feature means that there is less interchain coupling, i.e., less δ-type coupling between the t_{2g} orbitals of the same nature on W atoms bridged by the oxygen common to neighboring chains of octahedra (the degree of the coupling is governed by the tilt angle of the octahedra). The second feature means that there is less mixing between the chains, i.e., less hybridization between the t_{2g} orbitals of different nature in a given octahedron (the strength of the hybridization is governed by the distortion of this octahedron). All these features are those expected from the structural refinements[6] showing that the layers are made of more regular WO_6 octahedra when m increases.

With the above quoted decomposition of the total FS into partial FS's associated to the three types of chains, one can compute the average Fermi wave vector related to the filling of each type of chain. From Fig. 8 one gets $2k_F^a = 0.29(1)a^*$ for the chains **a** and $2k_F^d = 0.34(2)d_\pm^*$ for the chains **a**±**b** (the uncertainties take into account the warping of the FS). As the total number of electrons per chain is given by its $4k_F$ wave vector and as there is one chain **a** and two chains **a**±**b** per layer and two layers per unit cell, this leads to a total of $2(4k_F^a/a^*) + 4(4k_F^d/d_\pm^*) = 3.9 \pm 0.2$ conduction electrons per unit cell. This value, within experimental errors, accounts for the four electrons donated by the PO_4 groups. The average $2k_F^a$ value thus calculated for the 4/6 member, $0.29(1)a^*$, is closer to the $2k_F^a = 0.30(2)a^*$ value experimentally determined in the 6/6 member than that found, $0.33(2)a^*$, for the 4/4 member. This is the opposite situation for the $2k_F^d$ average value where that calculated for the 4/6 member, $0.34(2)d_\pm^*$, is closer to the $2k_F^d = 0.35(2)d_\pm^*$ value experimentally determined in the 4/4 member than those found $0.39(2)d_\pm^*$ and $0.38(2)d_\pm^*$ for the 6/6 member and 5/5 member, respectively.[8]

The difference of Fermi wave vectors between the 1D band structures originating from the $m=4$ and $m=6$ type layers is given by the splitting of their FS. From Fig. 8 it amounts to $\Delta 2k_F^a = 0.016a^*$ and $\Delta 2k_F^d = 0.03d_\pm^*$ for the chains **a** and **a**±**b**, respectively. These $2k_F$ differences lead to a charge transfer of about $\delta\rho \approx 0.08$ electrons between the $m=4$ and $m=6$ layers if one assumes that the outer and inner components of the FS shown in Fig. 8 belong to different layers (This hypothesis is sustained by the observation that the total FS of Fig. 8 exhibits hybridization gaps only when the partial FSs associated with the same layer cross). The sign of the charge transfer has not been determined. However one expects, because the network of octahedra is more regular in the $m=6$ layer than in the $m=4$ layer, that the t_{2g} levels will be of lower energy in the $m=6$ layer than the $m=4$ layer. This hypothesis agrees with photoemission measurements[26] which show that the binding energy of the t_{2g} levels increases when m increases. In that case one should have $2+\delta\rho$ electrons per segment of m octahedra in the $m=6$ layer and $2-\delta\rho$ electrons in the $m=4$ layers. With this interpretation both $2k_F^a$ and $2k_F^d$ increase from the $m=4$ layer to the $m=6$ layer. In the extended Huckel calculation of the electronic structure of the 4/6 member, performed in the hypothesis of no charge transfer between the layers,[27] there is a decrease of $2k_F^a$ and an increase of $2k_F^d$ from the $m=4$ layer to the $m=6$ layer, which is consistent with the sense of variation of $2k_F$ values observed in the regular m members.

By the presence of flat portions, the FS shown Fig. 8 exhibits remarkable nesting properties which must be at the origin of the structural instabilities exhibited by the 4/6 member. These properties will be considered in the following section in relationship with the discussion of the structural results.

V. DISCUSSION

A. The nesting instability and the T_{c1} transition

Figure 8 shows that the extremities of the $\mathbf{q}_1$ critical wave vector nest remarkably the flat portions of the FS, which form a lozenge around the X point of the Brillouin zone. In addition, the $\mathbf{q}_1$ wave vector, which is almost parallel to the edges of the lozenge, achieves a high degree of nesting between the edges linked by $\mathbf{q}_1$. This process leads to the nesting of the FS associated with the chains **a**±**b**. The $\mathbf{q}_1$ wave vector, as well as the $\mathbf{q}_2$ one, nest also approximately the FS associated with the chains **a**. According to Fig. 8 there is a difference of $0.04a^*$ ($=0.05$ Å^{-1}) between $2k_F^a = 0.29a^*$ of the average FS and the $q_a = 0.33a^*$ component of $\mathbf{q}_1$ and $\mathbf{q}_2$. This difference being comparable to the inverse CDW thermal coherence length on the chains **a** at T_{c1}, given by

$$\xi_{th}(T) = \frac{\hbar v_F}{\sqrt{2}\pi k_B T}, \tag{2}$$

and which amounts to $\xi_{th}^{-1}(T_{c1}) \simeq 0.04$ Å^{-1} from the results of $m/m = 4/4$,[10] the critical development of the CDW instability on the chains **a** is not inhibited by the misfit of the wave vectors. All these considerations show that the $\mathbf{q}_1$ structural transition is due to a CDW instability as in the other regular low-m members.[2] In addition, one expects, because of the quite good nesting properties of the lozenge parts of the FS, that the electron-hole response function will exhibit a stronger divergence in the $m/m = 4/6$ member than in the $m/m = 4/4$ member, which has less flat FS portions. This qualitatively explains why the CDW transition of the 4/6 member occurs at a critical temperature $T_{c1} = 156$ K, twice larger than that at $T_{c1} = 80$ K of the upper CDW transition of the 4/4 member for which a modulation at about the same wave vector is stabilized (see Table I).

Upon cooling, the thermal dependence of the transport properties[22] changes gradually above T_{c1} in a temperature range starting at about 180 K. This change could be explained by the formation of a pseudogap associated with the presence of sizable pretransitional fluctuations. In this condition the x-ray diffuse scattering investigation shows that interchain CDW correlations are present in a large temperature range extending to about 60 K above T_{c1}. The presence of such intralayer 2D correlations can be understood by the fact that when $\mathbf{q}_1$ remains parallel to the edges of the lozenge this is a best nesting of the FS and thus a maximum in the electron-hole response function. The increase of dimensionality of the pretransitional fluctuations could also explain the enhancement of the T_{c1} critical temperature in the 4/6 member with respect to that of the low-*m* regular members, which differently exhibit an important regime of 1D pretransitional fluctuations.

B. A two-order-parameter CDW transition

Curiously the transport measurements do not reveal the bump anomaly starting at T_{c1} observed in the $m/m=4/4$ member.[22] In addition, the decrease by a factor of 2 of the slope of the linear dependence of the thermopower[22] suggests that below T_{c1} the CDW modulation is only set in one layer out of two. The absence of a bump anomaly could thus be explained if gaps are only opened on the FS originating from the electronic wave functions of one layer and if the other layer remains metallic below T_{c1}. This implies that the nesting process considered in the preceding section connects in fact only half of the global FS, say, the FS associated with the m=6 layer (see Sec. III below). In this scenario only this layer becomes modulated at $T_{c1,}$ which thus sets the order parameter ρ_1. A suitable explanation of the thermal behavior of the transport properties and of the unusual variation of the intensity of the $\mathbf{Q}_1$ [Fig. 4(a)] and $\mathbf{Q}_2$ [Fig. 4(b)] satellite reflections can be simply provided if there is another order parameter ρ_2 which accounts for the CDW modulation of the other (say, $m=4$) layer, and whose thermal dependence is different from that of ρ_1. In the case of a single *q* modulation, these order parameters enter in the expression of the satellite intensity in the form

$$I(\mathbf{Q})=|\rho_1F_6(\mathbf{Q})+\rho_2F_4(\mathbf{Q})|^2\delta(\mathbf{Q}-\mathbf{G}\pm\mathbf{q}_1), \qquad (3)$$

where $F_m(\mathbf{Q})$ is the structure factor accounting for the modulation of the *m*th-type layer:

$$F_m(\mathbf{Q})=\sum_j f_j(\mathbf{Q})(\mathbf{Q}\cdot\mathbf{e}_j)\exp(i\mathbf{Q}\cdot\mathbf{r}_j),$$

and in which the atom *j* located in $\mathbf{r}_j$ and with atomic form factor $f_j(\mathbf{Q})$ is displaced with a polarization $\mathbf{e}_j$. In the expression (3) the large increase of the $\mathbf{Q}_1$ satellite intensity below T_{c1} reflects the rapid growth of ρ_1, while the increase of the $\mathbf{Q}_2$ satellite intensity below $T^*\simeq125$ K reflects the growth or a sizable increase of ρ_2. In the first situation, shown Fig. 9(a), which corresponds to the case where the ρ_1 and ρ_2 order parameters are of different symmetries, the two order parameters develop "independently" and regularly in temperature (in that case there is at lowest order a biquadratic coupling between ρ_1 and ρ_2). In the second situation, shown Fig. 9(b), which corresponds to the case where ρ_1 and ρ_2 have the same symmetry, the ρ_1 and ρ_2 order parameters appear at T_{c1}, then ρ_2 exhibits a rapid increase around T^* (in that case there is at lowest order a bilinear coupling between ρ_1 and ρ_2). The nonmonotonic variation of the satellite intensity at lower temperature can be explained by interference effects between the two contributions entering in Eq. (3) when the amplitudes of the two order parameters become equally important. $F_m(\mathbf{Q})$ being complex numbers, the magnitude of the interference effect also varies with the satellite position $\mathbf{Q}$ in reciprocal space.

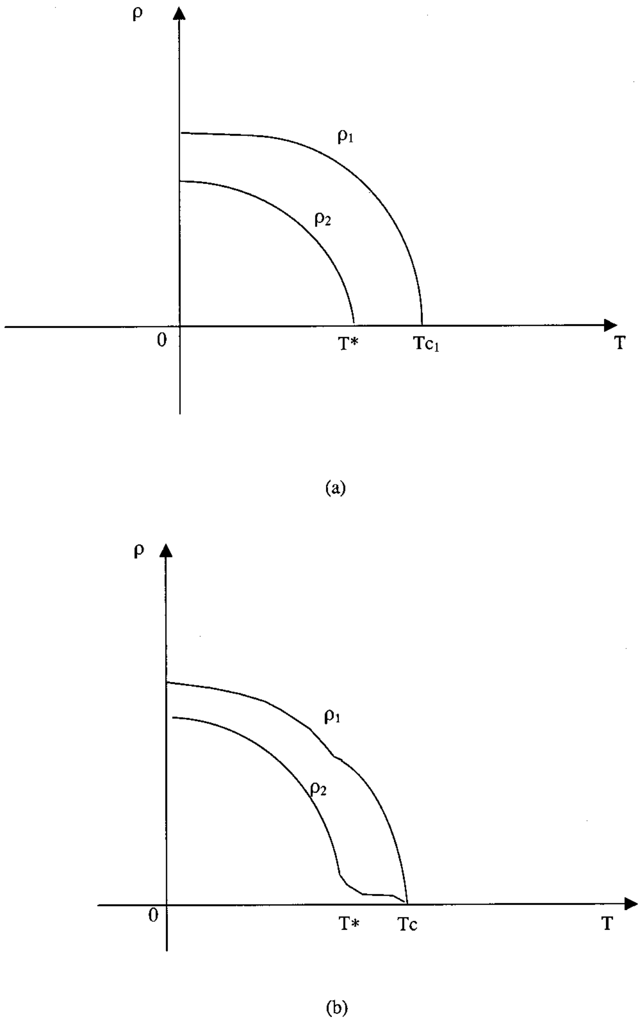

FIG. 9. Schematic representation of the thermal dependence of the two order parameters of the CDW transition of the 4/6 member in the case of ρ_1 and ρ_2 order parameters of different (a) and of same (b) symmetry.

C. A sliding modulation

As shown Fig. 6, the b^* component of the $\mathbf{q}_1$ wave vector varies in temperature principally between about 120 K ($\simeq T^*$) and 80 K ($\simeq T^{**}$). The sizable increase of the ρ_2 order parameter occurs at about the temperature T^*. This means that the start of the sliding of the $\mathbf{q}_1$ wave vector seems to be correlated with the growth of the ρ_2 modulation.

Under cooling, the modulus of $\mathbf{q}_1$ increases. In the FS nesting scenario considered in Sec. V A, this corresponds to a change of nesting from the inner lozenge centered at the *X* point of the Brillouin zone towards the outer lozenge. In Sec. IV we have provided evidences that the inner (outer) lozenge would correspond to the FS associated with the $m=6$ (m=4) layer. Thus from the sense of variation of the modulation wave vector one can justify the assertion previously made that the FS associated with the $m=6$ layer will be nested at T_{c1} and that the sliding of the modulation wave vector occurs in order to enhance the nesting with the FS associated with the $m=4$ layer. The best nesting will be achieved for a wave vector connecting one edge of the lozenge of the FS of the

$m=6$ layer to the opposite edge of the lozenge of the FS of the $m=4$ layer. According to the FS calculation of Fig. 8 this would lead to a variation of $0.03b^*$, assuming that the charge transfer between the layers does not change during the sliding of the CDW (see Sec. V D below). This number is relatively close to the experimental variation of $0.012(4)b^*$ for the total shift of Δq_{b^*} (Fig. 6). However the quality of the nesting must be appreciated on the total FS and not only on the lozenges around the X point. Finally, let us remark that the shift of the wave vector is less than the inverse of the CDW coherence length (estimated for the chains $\mathbf{a}\pm\mathbf{b}$ at $\xi_{th}^{-1}(T)\simeq 0.05$ Å^{-1}, in the temperature range T^*–T^{**}, from the data of the regular $m=4$ member,[10]) the sliding mechanism is not energetically prohibited. However the relationship between the sliding and the growth of the modulation on the $m=4$ layer must be clarified. This will be done using the phenomenology of the Landau-Ginzburg theory of the phase transitions in Sec V E below.

The nesting of the total FS is certainly completed around T^{**} when the thermal variation of $\mathbf{q}_1$ saturates and when the thermal variation of the thermopower deviates from the linear behavior expected in a metallic state. Magnetotransport measurements at low temperature[22] show, by the detection of small electron and hole pockets, that a quite good nesting is achieved. Thus the sliding of the modulation wave vector renders the 4/6 member semimetallic. The same electronic ground state is achieved in the other low-m regular members by a different mechanism in which successive CDW transitions are set.[2,3] As the 4/6 member is made of different layers, the sliding of the nesting wave vector is probably the most economic way to achieve a semimetallic state. The gradual appearance of a semimetallic state in temperature via a sliding modulation mechanism probably explains why the resistivity of the 4/6 member does not exhibit the bump anomaly observed in the regular m members at their successive CDW transitions.

D. Comparison with other quasi-1*D* systems made of two types of metallic chains differently filled

It is interesting to compare our findings in the 4/6 member with the results previously obtained in quasi-1D conductors made with spatially separated chains for the purpose of determining in which condition a CDW instability can be set in the presence of two different 1D electron gases having, respectively, the $2k_F^{\mathrm{I}}$ and $2k_F^{\mathrm{II}}$ critical wave vectors.

A first family of materials which has been extensively studied is the charge-transfer salts made of segregated stacks of donors and acceptors.[28] But in most of them the number of electrons on the acceptor stack amounts to the number of holes on the donor stack, which implies $2k_F^{\mathrm{I}}=2k_F^{\mathrm{II}}$ within one reciprocal-lattice wave vector. However, TTF-TCNQ is particularly interesting because after a $2k_F^{\mathrm{I}}$ CDW order which develops on the TCNQ sublattice, the development of the $2k_F^{\mathrm{II}}$ CDW on the TTF sublattice at lower temperature leads to the sliding of the transverse component of the modulation (in the direction where the TCNQ and TTF stacks alternate). The growth of the amplitude of the modulation on the TTF stacks controls the transverse shift of wave vector.[29] In addition, the interchain CDW order in this direction improves on cooling with the growth of the TTF order parameter and thus with the increase of the interchain coupling.[30] It is thus interesting to remark that the opposite behavior occurs in the 4/6 member, where the CDW order in the $\mathbf{c}^*$ interlayer direction degrades on cooling.

A second family of materials is the transition-metal trichalcogenides.[31] Monoclinic NbSe$_3$ and TaS$_3$ crystallize with two different types of conducting chains (called types I and III in the literature) with slightly different band filling (i.e., $2k_F$ wave vectors). Although the $2k_F^{\mathrm{I}}-2k_F^{\mathrm{II}}$ difference is quite small ($0.018b^*$ and $0.006b^*$ in NbSe$_3$ and TaS$_3$, respectively) and is comparable to the $2k_F$ difference between chains located on the $m=4$ and 6 layers of the 4/6 member (see Sec. IV), two successive and independent CDW transitions corresponding to different transverse CDW orders, each affecting a given sublattice of chains, are observed.[31] The orthorhombic variety of TaS$_3$ is more interesting because the CDW modulation wave vector varies in temperature and saturates at a commensurate value at low temperature.[32] The behavior bears some resemblance with that shown by the 4/6 member. However the chain array of the orthorhombic structure is so imperfectly known so that a detailed theory cannot be built.

Several theories[33–36] have considered the case of a CDW instability on two Peierls chains with nearly equal $2k_F$ wave vectors. In three of them[33–35] the problem has been analyzed in the limit of very strongly coupled CDW's: the relative phase between the CDW located on the two types of chains is then fixed and there is a single lattice deformation (i.e., a single order parameter). The deformation can be described by a lattice of amplitude solitons. Each band exhibits two energy gaps with a midgap subband built by the soliton electronic states. When the gap (i.e., the order parameter) increases, the periodicity of the soliton lattice decreases. When the gap becomes larger than the band splitting ($\hbar v_F|k_F^{\mathrm{I}}-k_F^{\mathrm{II}}|$) the deformation acquires a sinusoidal shape with the $k_F^{\mathrm{I}}+k_F^{\mathrm{II}}$ critical wave vector. In parallel, there is a continuous electron transfer between the two bands which terminates when both bands are equally filled. This description with only a single order parameter does not correspond to the situation observed in the 4/6 member.

When there is a weak bilinear coupling between the CDW on chains I and II (for example, due to the direct Coulomb coupling between the CDW's), their relative phase is no longer fixed and two lattice deformations or order parameters (one per chain) must be considered. This is a quite difficult problem to solve because generally a charge transfer between the two types of chains accompanies the relative growth of the order parameters. A simplified solution is given in Ref. 36. The three types of solutions found are summarized in the Appendix. They have some relevance with our findings for the $m/m=4/6$ bronze, as we shall see in the following section. The interesting point of the theory of Ref. 36 is that any local variation of $2k_F$, which leads to a shift of π of the phase of the modulation, generates a discommensuration that bears a net electric charge of e.[40]

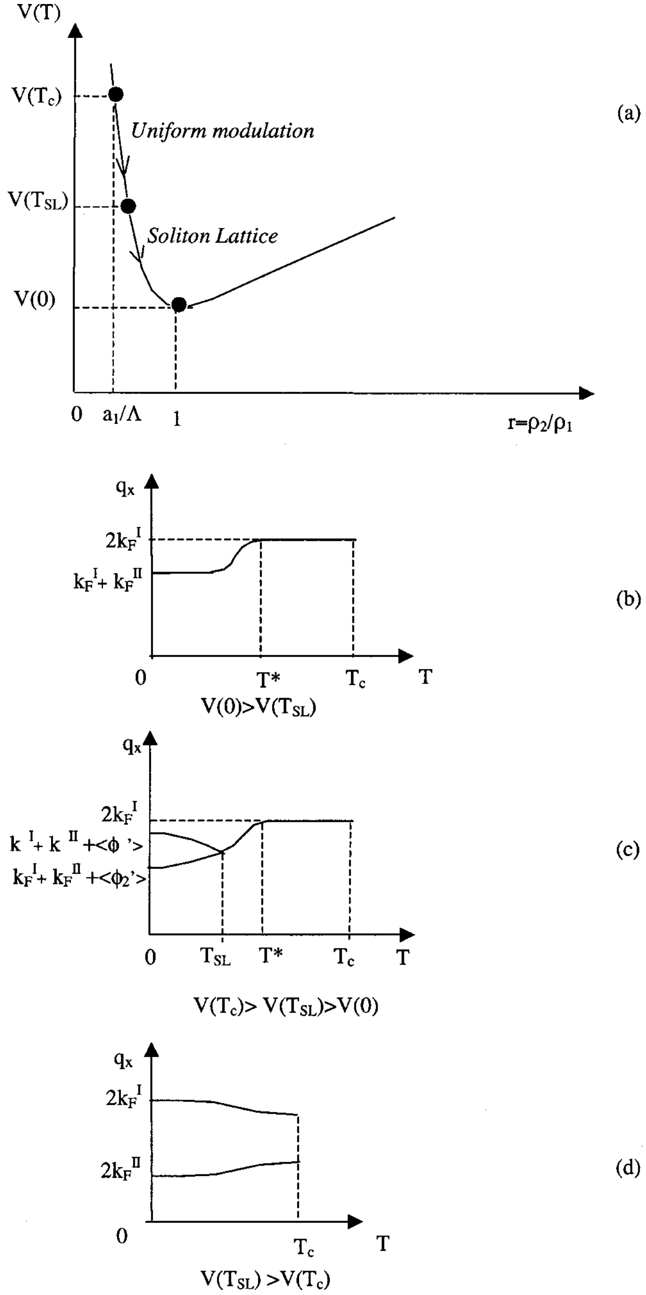

FIG. 10. (a) Variation of the potential $V(r)$ as a function of $r=\rho_2/\rho_1$. The situation depicted corresponds to the case (c). Schematic representation of the thermal variation of the wave vector q_x of the main reflection(s) of the Peierls modulated chains for (b) $V(0\ \mathrm{K})>V(T_{SL})$, (c) $V(T_c)>V(T_{SL})>V(0\ \mathrm{K})$, and (d) $V(T_{SL})>V(T_c)$.

E. A disordered dilute soliton lattice in the 4/6 member?

Several basic ingredients of Bjelis and Barisic's theory[36] are observed in the CDW modulation of the 4/6 member: the presence of two order parameters (Sec. V B), a sliding modulation which saturates at low temperature (Sec. V C). But the main characteristic of a soliton lattice (SL) consisting in the presence of sideband satellite reflections (Figs. 11 and 12) is not observed. However if the discommensurations are disordered it would be difficult to observe the sidebands, but instead one should observe a broadening of the satellite reflection, especially in the **b*** direction of the sliding of the modulation. A broadening of the $\mathbf{q}_1$ main satellite reflection, in excess of the experimental resolution (of 6×10^{-3} Å^{-1}, half-width at half maximum), is however not observed in the (a^*,b^*) reciprocal plane. This means that if a SL is present

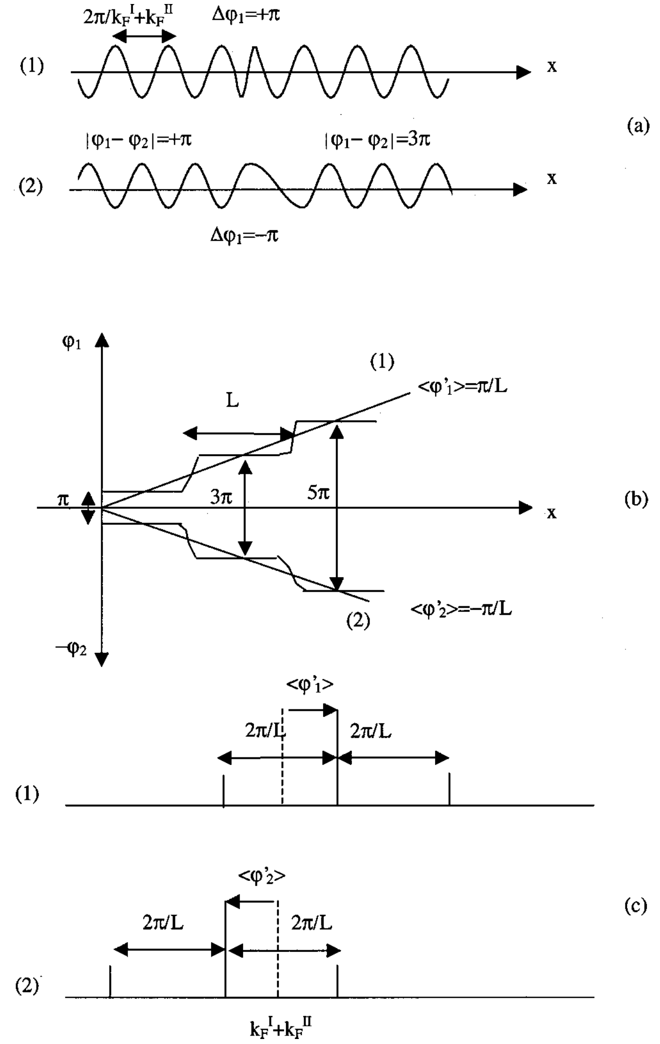

FIG. 11. (a) Spatial representation of the soliton lattice in the relative phase of the CDW located on chains 1 and 2. (b) Spatial variation of their phase φ_i and (c) Fourier transform of their individual modulation.

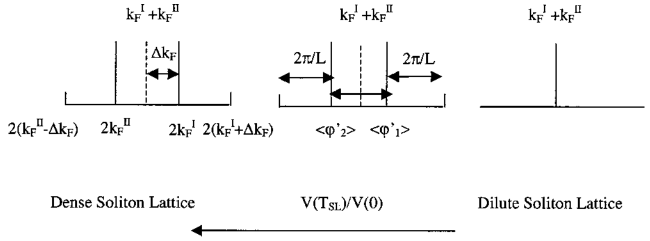

FIG. 12. Diffraction pattern of the modulated Peierls chains as a function of the ratio $V(T_{SL})/V(0\ \mathrm{K})$. When this ratio increases the separation between the sidebands increases and the soliton domain length L decreases.

at low temperature, it must be relatively diluted. Another possibility is that the coupling between CDW's would be strong enough to keep the modulation sinusoidal. This will correspond to the situation depicted in Fig. 10(b). In that case the expression (A7), taken from the Landau-Ginzburg theory given in the Appendix, can account quite well for the thermal variation of the modulation wave vector. This last expression clearly shows that the sliding of the wave vector is related to the relative growth of the ρ_2 order parameter on the $m=4$ layer, through the ratio $r=\rho_2/\rho_1$. It explains (i) the nonvariation of the wave vector above T^* when ρ_2 is not enough developed, (ii) the rapid variation of the wave vector at temperature below T^* when ρ_2 increases strongly, and (iii) the low-temperature saturation at the wave vector $k_F^{\mathrm{I}}+k_F^{\mathrm{II}}$ when the ratio r tends to 1. All this behavior relies also on the microscopic mechanism of a progressive nesting as proposed in Sec. V C.

In fact it is very difficult to discriminate between a dilute SL and a sinusoidal modulation, which corresponds to the limit where the separation between the discommensurations becomes very large. Such a distinction will be even more difficult to do in presence of disorder in the SL. In this situation only local measurements could reveal the presence of a dilute and/or disordered discommensuration lattice.

However, according to our results, two aspects of the modulated structure of the 4/6 member seem to indicate the presence of a dilute SL. The first one is that the pinning of discommensurations by the local minima of the potential provides a simple explanation of the hysteresis phenomena observed below T^* between the cooling and heating cycles of measurement of the satellite intensity (Fig. 4). The second feature concerns the broadening upon cooling of the $\mathbf{q}_1$ satellite reflections along $\mathbf{c}^*$ (Fig. 7), which should have a natural explanation in the presence of a low-temperature (disordered?) lattice of discommensurations. In that case, the regions where the amplitude or the phase of the CDW modulation remains not spatially uniform, as in the discommensurations, are the weak links in the interchain coupling. Any kind of randomness in the repeat periodicity of the discommensuration lattice, should drive an interchain disorder. In addition, the increase amount of discommensurations upon cooling would explain the observed enhancement of the interchain disorder.

The profile of the satellite reflection in the transverse direction, z, is proportional to the displacement-displacement correlation function

$$\langle |u(q_x+\delta q_z)|^2\rangle = \sum_{pm} \langle u_p(x)u_m^*(x)\rangle \exp(id_{pm}\delta q_z), \quad (4)$$

where $u_p(x)$ is the lattice modulation, given by Eq. (A1), in the pth chain (layer) and d_{pm} is the distance between the pth and mth chains (layers). On the right-hand side of Eq. (4) the average is performed in the chain (layer) direction, x. If the disorder originates from the randomness in the relative phase of the modulation between successive chains (layers), the interchain dependence of $\langle u_p(x)u_m^*(x)\rangle$ will be given by

$$\langle\langle \exp[i(\varphi_p-\varphi_m)]\rangle\rangle \approx \exp(-d_{pm}/l), \quad (5)$$

where on the left-hand side of Eq. (5) there is a second average on the chain (layer) taken at the origin. The exponential decay in the right member of Eq. (5) is the one experimentally deduced from the Fourier transform of the profile of the satellite reflections of the 4/6 member, as seen in Sec. III B 2 (l being the length of the coherent domains). Many models of disorder in 1D leads to an exponential decay of the correlation function. For example, (1) if there is a random distribution of domain size, with μ being the probability to cross a domain wall per unit length, it is easy to show,[37] if the phase coherence is completely lost on crossing a domain wall, that

$$l=\mu^{-1} \quad (6)$$

and (2) if there are random phase jumps of α, in linear concentration n, one gets after some calculation[38]

$$l=[n(1-\cos\alpha)]^{-1}. \quad (7)$$

In these models the decrease of l upon cooling comes from the increase of μ or n (and α). In particular, μ or n should increase with the linear density of discommensurations. More precisely the interchain (interlayer) order in the SL limit implies, as shown in Fig. 11, the simultaneous presence of discommensurations, which assure opposite phase jumps of $\pm\pi$ on neighboring chains (layers). If this does not occur, a defect, where a phase shift of $\alpha=+\pi$ or $-\pi$ is lacking, will be generated. In that case, the expression (7) reduces to $l=(2n)^{-1}$. For chains (layers) of discommensurations randomly distributed along z one has $n\approx 1/L$ times a geometrical factor (L is the mean length between discommensurations, as defined in Fig. 11). This geometrical factor is estimated at about $2b/c$ in the 4/6 member (b is the lattice periodicity in the direction of the layer where the wave vector slides and $c/2$ is the interlayer periodicity). Assuming a fully developed SL with $\langle\varphi'\rangle=\pi/L=\Delta k_F$, one gets $l\approx\pi c/4b\Delta k_F$. If one takes Δk_F equal to the range of sliding of the wave vector, $0.012b^*$, one obtains $l\approx 200$ Å, which is relatively close to the experimental value of 120 Å at 25 K.

In fact the 4/6 member develops a CDW modulation pattern, which is more complex than that considered for the purely 1D two-chain systems because (1) the $\mathbf{q}_1$ CDW modulation wave vector has two nonzero components in the conducting layer and (2) the local displacement pattern could be the superimposition of two modulation waves with, respectively, the $\mathbf{q}_1$ and $\mathbf{q}_1'$ wave vectors, as seen in Sec. III A 2. The observation of weak $\mathbf{q}_2$ satellite reflections ($2\mathbf{q}_2=\mathbf{q}_1+\mathbf{q}_1'$), up to at least T^*, suggests that the two modulations are simultaneously present in the same domain. In that case if one assumes that each modulation occurs with the same amplitude u_0, the modulation pattern of a given layer can be expressed in the form

$$u(\mathbf{r})=u_0[\cos(\mathbf{q}_1\cdot\mathbf{r}+\psi)+\cos(\mathbf{q}_1'\cdot\mathbf{r}+\psi')],$$

$$u(\mathbf{r})=2u_0\{\cos[\mathbf{q}_2\cdot\mathbf{r}+(\psi+\psi')/2]\cos[(\mathbf{q}_1-\mathbf{q}_1')\cdot\mathbf{r}/2 +(\psi-\psi')/2]\},$$

$$u(\mathbf{r})=2u_0\{\cos[2\pi x/3+(\psi+\psi')/2]\cos[2\pi y/3+y\Delta q_{b*}b+(\psi-\psi')/2]\}. \tag{8}$$

This pattern corresponds to commensurate CDWs running along the chains **a** (coordinate x), the amplitude of which is incommensurately modulated in the **b** direction (coordinate y). It is along **b**, where the modulation wavelength varies in temperature, that the SL previously considered could form. As the amplitude of the CDW's strongly varies in the **b** direction, the discommensuration lines should be oriented perpendicularly to this direction or along the segment direction. The presence of such a complex SL does not change the main conclusions of the interpretation given in this section.

F. The $\mathbf{q}_2$ modulation

At the present stage of our investigation, two possibilities remains open to account for the observed weak $\mathbf{q}_2$ satellite reflections. The first possibility is that $\mathbf{q}_2$ corresponds to a two-CDW instability involving chains **a** because its nonzero $\mathbf{a}^*$ component could approximately nest the FS associated with chains **a**, as seen in Sec. V A. The second possibility considered at the end of Sec. V E is that $\mathbf{q}_2$ corresponds to a side effect of the $\mathbf{q}_1$ and $\mathbf{q}_1'$ modulations; these last modulation involves the chains $\mathbf{a}\pm\mathbf{b}$ as seen in Sec. V A.

VI. CONCLUSION

The alternate 4/6 member stabilizes CDW modulations whose $\mathbf{q}_1$ and $\mathbf{q}_2$ critical wave vectors are very close to those found in the low-m regular members (Table I). As these wave vectors are fixed by the FS nesting mechanism, the topology of the FS remains very close in all these members. However the CDW transitions, which all achieve a low-temperature semimetallic state, do not proceed in the same manner in the regular and alternate members. In the regular member it proceeds by setting successive second-order Peierls-like transitions, which successively stabilizes different intralayer "hidden" nesting wave vectors along the sequence $\mathbf{q}_1$ then $\mathbf{q}_2$ in the $m=4$ and 5 members or along the reverse sequence $\mathbf{q}_2$ then $\mathbf{q}_1$ in the $m=6$ member. In the alternate 4/6 member the $\mathbf{q}_1$ critical wave vector is stabilized at high temperature by the nesting of the FS of the $m=6$ layer, then this wave vector progressively slides in order to nest also the FS of the $m=4$ layer.

We have accounted for the thermal variation of the $\mathbf{q}_1$ modulation wave vector of the 4/6 member using a model[36] derived from the Landau-Ginzburg theory of the phase transitions in which the relative phase between CDW located on structurally different layers can vary, and where the charges transferred between the layers could nucleate discommensurations. We suggest that a disordered and dilute SL could result of such a mechanism.

Such an interpretation could also be invoked for $m\geqslant 7$ members, where the amount of intergrowth defects increases with m and the conditions of preparation of the sample.[41] In relationship with the study of the 4/6 member it is tempting to suggest that the intergrowth defects could lead to local charge transfers between adjacent layers of different m values. It would result a smeared FS exhibiting a distribution of $2k_F$ values, the broadening of which will smoothen its nesting properties and thus the divergence of the associated electron-hole response function. However, a local CDW order could remain present in these disordered bronzes. Thus, by analogy with the findings in the 4/6 member, we suggest that discommensurations could be nucleated on the charges transferred at the level of the intergrowth defects, breaking the long-range CDW order observed in the defect-free bronzes. Moreover, a dense and disordered discommensuration lattice has been effectively imaged by electron microscopy in the $m=12$ bronze doped with Ge.[39] The presence of such nucleated discommensurations on stacking faults provides a suitable explanation for many observations performed in the $m\geqslant 7$ members, where the quality of the CDW diffraction pattern (i.e. number of harmonics of modulation, thickness of the satellite reflections) depends on the samples probably through its amount of stacking faults). Such charged defects should perturb considerably the electronic properties of these large-m members and be invoked to explain their electronic properties.[15]

APPENDIX

The results of the calculation of Ref. 36 can be summarized in the following way. If one writes the lattice deformation in chain direction, x, for the two types ($i=1,2$) of chains in the form

$$u_i(x)=\rho_i\ \exp[i(k_F^{\mathrm{I}}+k_F^{\mathrm{II}})x]\exp(i\varphi_i), \tag{A1}$$

the Landau-Ginzburg expansion of the free energy, in q space, for bilinearly coupled chains (by Λ) can be put under the standard form

$$F(q)=F_1(q)+F_2(q)+F_{1,2}(q) \tag{A2}$$

with

$$F_i(q)=a_i(T)\rho_i^2+b_0\rho_i^4+a_0\xi_0^2[(\rho_i')^2+\rho_i^2(\varphi_i'\pm\Delta k_F)^2],$$

$$F_{1,2}(q)=2\Lambda\rho_1\rho_2\cos(\varphi_1-\varphi_2),$$

and $\Delta k_F=k_F^{\mathrm{I}}-k_F^{\mathrm{II}}$, which will be taken to be greater than 0 below.

In these expressions the prime means a spatial derivative. In the gradient term ξ_0 is the CDW coherence length defined by expression (1) or (2). We shall also neglect the possibility of interchain electron charge transfer when the CDW modulation develops, which means that Δk_F remains constant in temperature (the interchain charge transfer, also considered in Ref. 36, will not change the nature of the solutions but their domain of stability will be modified).

If one sets $\varphi_1=\gamma+\beta$ and $\varphi_2=\gamma-\beta$ the minimization of F with respect to γ gives

$$\gamma'=-(1-r^2)(1+r^2)^{-1}(\beta'-\Delta k_F), \tag{A3}$$

where $r=\rho_2/\rho_1$ and

$$F(q)=\Phi_1(q)+\Phi_2(q)+\Phi_{1,2}(q) \tag{A4}$$

with

$$\Phi_i(q)=a_i(T)\rho_i^2+b_0\rho_i^4+a_0\xi_0^2(\rho_i')^2,$$

$$\Phi_{1,2}(q)=\rho_2^2(1+r^2)^{-1}[4a_0\xi_0^2(\beta'-\Delta k_F)^2 +2\Lambda V(r)\cos 2\beta].$$

where $V(r)=r+r^{-1}$.

$\Phi_{1,2}(q)$ is a sine-Gordon equation. The minimum of its kinetic-energy term, which occurs for $\beta'=\Delta k_F$ (i.e., $\beta=\Delta k_F x+cte$), tends to promote the natural $2k_F$ wave vector of each chain and thus the ordering of CDW with different wave vectors. Its bilinear coupling term tends to promote the ordering of a unique CDW of mean wave vector. In this latter term, the phase shift $2\beta=\pi$ (for $\Lambda>0$) between CDW minimizes the interchain coupling energy, which is generally of Coulomb origin. In the free energy, one sets, as usual,

$$a_i(T)=a_0(T/T_{ci}-1). \tag{A5}$$

As $T_{c1}>T_{c2}$, ρ_2 will be less than ρ_1 in the whole temperature range, thus $r\leqslant 1$. The behavior of the two order parameters is shown in Fig. 9(b), with T_c given by $a_1(T_c)a_2(T_c)\approx\Lambda^2$ and $T^*\approx T_{c2}$. When T increases, r increases and thus $V(r)$ decreases, as shown in Fig. 10(a). The nature of the solution which minimizes the free energy depends upon the ratio of the cost of elastic distortion energy to create discommensurations over the gain of interchain coupling energy to form domains with the same modulation:

$$V(T_{SL})=a_0(\xi_0^2\Delta k_F\pi/2)^2/\Lambda. \tag{A6}$$

Depending on the value of $V(T_{SL})$ with respect to $V(T_c)\approx a_1/\Lambda$ and $V(0\ \text{K})=2$ three cases must be considered.

(i) $V(0\ \text{K})>V(T_{SL})$ [Fig. 10(b)], which corresponds to the limit of strong coupling between CDW's (large Λ). The bilinear coupling term is always dominant in the sine-Gordon equation. One has, with $\beta=\pi/2$ in the whole temperature range, a sinusoidal modulation. With $\beta'=0$, the common modulation wave vector is given, from the expression (A3), by

$$q_x=k_F^{\mathrm{I}}+k_F^{\mathrm{II}}+\gamma' \tag{A7}$$

with $\gamma'=\varphi_1'=\varphi_2'=(1-r^2)(1+r^2)^{-1}\Delta k_F$.

Its rate of variation depends upon r: it is small between T_c and T^* when r is weak, strong just below T^* when r increases, then it saturates to zero at low temperature if $r\rightarrow 1$.

(ii) $V(T_{SL})>V(T_c)$ [Fig. 10(d)], which corresponds to the limit of weak coupling (Λ). The CDW's are nearly decoupled. The kinetic-energy term is dominant in the sine-Gordon equation. Each CDW tends to stabilize its own $2k_F$ wave vector. The SL already appears at T_c. In the limit $\Lambda\rightarrow 0$ one has $\beta'=\varphi_1'=-\varphi_2'=\Delta k_F$ and thus $\gamma'=0$.

(iii) $V(T_c)>V(T_{SL})>V(0\ \text{K})$ [Fig. 10(c)], which corresponds to Coulomb couplings between CDW's of intermediate strength. There is a uniform modulation between T_c and T_{SL} and a SL develops below T_{SL}.

Figure 11(a) represents schematically, in the real space, such a SL in the relative phase 2β between the two types of CDW. It is composed of domains of length L, with the common modulation wave vector $k_F^{\mathrm{I}}+k_F^{\mathrm{II}}$, separated by discommensurations where the phase φ_i of each type of chain simultaneously experiences jumps of $+\pi$ and $-\pi$ in such a way to keep a relative phase shift of $2\beta=(2p+1)\pi$ between the chains (p is an integer), as shown Fig. 11(b). At a phase jump of $\pm\pi$ must be associated a charge of $\pm e$.[40] The spatial average of the $2k_F$ wave vector of each chain is thus given by $k_F^{\mathrm{I}}+k_F^{\mathrm{II}}+\langle\varphi_i'\rangle$, with $\langle\varphi_i'\rangle=-\langle\varphi_2'\rangle=\pi/L$ (the natural $2k_F^{\mathrm{I}}$ and $2k_F^{\mathrm{II}}$ wave vectors are recovered for a dense SL when $\pi/L=\Delta k_F$ in the limit $\Lambda\rightarrow 0$). The wave vector in excess of $k_F^{\mathrm{I}}+k_F^{\mathrm{II}}$ on chain 1 forms $+\pi$ discommensurations, corresponding to charges $+e$, while the wave vector in defect of $k_F^{\mathrm{I}}+k_F^{\mathrm{II}}$ on chain 2 forms $-\pi$ discommensurations, corresponding to charges $-e$. The conservation of the total number of electrons between the two kinds of chains requires an equal amount of $+e$ and $-e$ charges. The minimization of interchain Coulomb energy requires that a charge $+e$ on a given chain will be surrounded by a charge $-e$ on the neighboring chain and thus that opposite discommensurations face each other, as shown in Fig. 11(b), in order to keep locally the charge neutrality.

The Fourier transform of the SL, shown in Fig. 11(c), consists of two main reflections at the average $2k_F$ wave vector of each chain surrounded by sidebands of satellite reflections having the reciprocal periodicity $\pm n2\pi/L$ (n is an integer) of the lattice of discommensurations. The sidebands are due to the intermodulation of the natural periodicity of one chain by the natural periodicity of the other chain.

Figure 12 summarizes the evolution of the diffraction pattern of the modulated Peierls chains in its ground state as a function of $V(T_{SL})/V(0\ \text{K})$. The density of discommensurations increases when $V(T_{SL})/V(0\ \text{K})$ increases. Since $V(T_{SL})/V(r)$ decreases when the temperature increases one expects a continuous evolution of the diffraction pattern with T, analogous to that shown by Fig. 12 when $V(T_{SL})/V(0\ \text{K})$ decreases. On that basis we have represented in Figs. 10(b–d), the expected variation of the wave vector of the main reflections of the modulated chain for the three cases considered previously. In this figure we have assumed a continuous evolution of q_x in temperature between 0 K and T_c. However the determination of $q_x(T)$ requires the minimization of the total free energy, which remains to be done in the general case.

---

[1] C. Schlenker, *Low-Dimensional Electronic Properties of Molybdenum Bronzes and Oxides*, edited by (Kluwer Academic, Dordrecht, 1990).

[2] Int. J. Mod. Phy. B **23–24** (1993).

[3] *Physics and Chemistry of Low Dimensional Inorganic Conductors, Vol. 354 of NATO Advanced Studies Institute, Series B: Physics*, edited by C. Schlenker, J. Dumas, M. Greenblatt, and S. van Smaalen, (Plenum, New York, 1996).

[4] Y. Ueda, Chem. Mater. **10**, 2653 (1998).

[5] M. Whangbo, E. Canadell, P. Foury, and J.-P. Pouget, Science **252**, 96 (1991).

[6] P. Roussel, O. Perez, and Ph. Labbé, Acta Crystallogr., Sect. B: Struct. Crystallogr. Cryst. Chem. **57**, 603 (2001).

[7] A. Benmoussa, Ph. Labbé, D. Groult, and B. Raveau, J. Solid State Chem. **44**, 318 (1982).

[8] P. Roussel, P. Foury-Leylekian, B. Domenges, D. Groult, Ph. Labbé, and J.-P. Pouget, Eur. Phys. J. B **12**, 497 (1999).

[9] E. Canadell and M.H. Whangbo, Chem. Rev. **91**, 965 (1991); *Physics and Chemistry of Law Dimensional Inorganic Conductors*, Int. J. Mod. Phys. B **23–24**, 4005 (1993); Ref. 3, p. 271.

[10] E. Sandré, P. Foury-Leylekian, S. Ravy, and J.-P. Pouget, Phys. Rev. Lett. **86**, 5100 (2001).

[11] K. Breuer, C. Stagarescu, K.E. Smith, M. Greenblatt, and K. Ramanujachary, Phys. Rev. Lett. **76**, 3172 (1996); G.-H. Gweon, J.W. Allen, J.A. Clack, Y.X. Zhang, D.M. Poirier, P.J. Benning, C.G. Olson, J. Marcus, and C. Schlenker, Phys. Rev. B **55**, R13 353 (1997).

[12] P. Foury and J.P. Pouget, Int. J. Mod. Phys. B **23-24**, 3937 (1993).

[13] C. Schlenker, C. Hess, C. Le Touze, and J. Dumas, J. Phys. I **6**, 2061 (1996).

[14] M. Greenblatt, Acc. Chem. Res. **29**, 219 (1996).

[15] J. Dumas, C. Hess, C. Schlenker, G. Bonfait, E. Gomes Marin, D. Groult, and J. Marcus, Eur. Phys. J. B **14**, 73 (2000).

[16] A. Ottolenghi and J.-P. Pouget, J. Phys. I, **6**, 1059 (1996).

[17] C. Hess, C. Schlenker, G. Bonfait, T. Ohm, C. Paulsen, J. Dumas, Z.S. Teweldemedhin, M. Greenblatt, J. Marcus, and M. Almeida, Solid State Commun. **104**, 663 (1997).

[18] P. Roussel, Ph. Labbé, H. Leligny, D. Groult, P. Foury-Leylekian, and J.-P. Pouget, Phys. Rev. B **62**, 176 (2000).

[19] C. Schlenker, C. Le Touze, C. Hess, A. Rötger, J. Dumas, J. Marcus, M. Greenblatt, Z.S. Teweldemedhin, A. Ottolonghi, P. Foury, and J.-P. Pouget, Synth. Met. **70**, 1263 (1995).

[20] C. Hess, A. Ottolenghi, J.-P. Pouget, C. Schlenker, J.L. Hodeau, and J. Marcus, Synth. Met. **86**, 2169 (1997).

[21] W.L. McMillan, Phys. Rev. B **16**, 643 (1977).

[22] U. Beierlein, C. Hess, C. Schlenker, J. Dumas, R. Buder, D. Groult, E. Steep, D. Vignolles, and G. Bonfait, Eur. Phys. J. B **17**, 215 (2000).

[23] P. Foury, P. Roussel, D. Groult, and J.-P. Pouget, Synth. Met. **103**, 2624 (1999).

[24] M.C. Payne, M.P. Teter, D.C. Allan, and J.D. Joannopoulos, Rev. Mod. Phys. **64**, 1045 (1992).

[25] R.W. Nunes and D. Vanderbilt, Phys. Rev. B **50**, 12 025 (1994).

[26] N. Witkowski, M. Garnier, D. Purdie, Y. Baer, D. Malterre, and D. Groult, Solid State Commun. **103**, 471 (1997).

[27] I. I. Rachidi, Thesis Universitéd'Orsay, France, 1989).

[28] J.-P. Pouget, *Highly Conducting Quasi-One-Dimensional Organic Crystals*, edited by E. Conwell, Semiconductors and Semimetals Vol. 27 (Academic Press, New York, 1988), Chap. 3.

[29] P. Bak and V.J. Emery, Phys. Rev. Lett. **36**, 978 (1976).

[30] J.-P. Pouget, S.M. Shapiro, G. Shirane, A.F. Garito, and A.J. Heeger, Phys. Rev. B **19**, 1792 (1979).

[31] P. Monceau, in *Electronic Properties of Inorganic Quasi One Dimensional Materials II*, edited by P. Monceau (Reidel, Dordrecht, 1985), p. 139. In the monoclinic variety, two CDW's cannot be coupled through the lowest (bilinear) term considered in Ref. 37 to achieve a common CDW $2k_F$ modulation because of different transverse components of their wave vector.

[32] C. Roucau, J. Phys. Colloq. **44**, C3-1725 (1983).

[33] S.A. Brazovskii, I.E. Dzyaloshinskii, and N.N. Kirova, Sov. Phys. JETP **54**, 1209 (1981).

[34] S.A. Brazovskii and S.I. Matveenko, Sov. Phys. JETP **60**, 804 (1984).

[35] C. Noguera, J. Phys. C **19**, 2161 (1986).

[36] A. Bjelis and S. Barisic, J. Phys. C **19**, 5607 (1986).

[37] P. Debye, M.R. Anderson, and M. Brumberger, J. Appl. Phys. **28**, 679 (1957).

[38] S. Ravy (unpublished).

[39] Y. Yan, M. Kleman, C. Le Touze, J. Marcus, C. Schlenker, and P.A. Buffat, Europhys. Lett. **30**, 49 (1995).

[40] The charge included in a wavelength $\lambda_F=\pi/k_F$, or in a phase difference of 2π, of a $2k_F$ CDW is $2e$ If a is the chain periodicity and if there are n_0 electrons per site, the number of conduction electrons included in a CDW wavelength is $n_0\lambda_F/a$, which amounts to 2 when the relationship $\lambda_F=2a/n_0$ is used (the factor 2 in this last expression accounts for the spin degeneracy). Thus in a $2k_F$ CDW, one electron corresponds to a phase shift of π.

[41] B. Domengès, P. Roussel, Ph. Labbé, and D. Groult, J. Solid State Chem. **127**, 302 (1996).